The study of chromium oxide loading on platinum chromium oxide zirconia catalyst for *n*-dodecane and 1,4-diisopropylbenzene hydrocracking

IOP Conf. Series: Materials Science and Engineering **736** (2020) 042039 doi:10.1088/1757-899X/736/4/042039

The study of chromium oxide loading on platinum chromium oxide zirconia catalyst for *n*-dodecane and 1,4-diisopropylbenzene hydrocracking

N H R Annuar[1,*], L P Teh[2], H D Setiabudi[3,4], M A A Aziz[5], N M Salam[6], A A Jalil[5,7]

[1] Department of Chemistry, Faculty of Applied Sciences, Universiti Teknologi MARA (UiTM) Johor, Pasir Gudang Campus, 81750 Masai, Johor, Malaysia.
[2] Faculty of Science and Technology, Universiti Kebangsaan Malaysia, 43600 UKM Bangi, Selangor, Malaysia.
[3] Faculty of Chemical and Natural Resources Engineering, [4] Centre of Excellence for Advanced Research in Fluid Flow, Universiti Malaysia Pahang, 26300 Gambang, Kuantan, Pahang, Malaysia.
[5] School of Chemical and Energy Engineering, Faculty of Engineering, [6] Department of Chemistry, Faculty of Science, [7] Centre of Hydrogen Energy, Institute of Future Energy, Universiti Teknologi Malaysia (UTM), 81310 UTM Johor Bahru, Johor, Malaysia
*Corresponding author: nurha8558@uitm.edu.my

Abstract. Hydrocracking reaction is one of the major processes in petroleum refining. To date, the exploration of a suitable catalyst for hydrocracking reaction remains challenging. The presence of Pt loaded on Cr_2O_3-ZrO_2 promotes the catalytic activity and stability of Cr_2O_3-ZrO_2. While, zirconia has an interesting thermal and mechanical properties which make it as a support material. Therefore, in this study, platinum chromium oxide zirconia catalyst (Pt/Cr_2O_3-ZrO_2) with different Cr_2O_3 loading (1, 4, 8, and 12 wt%) were prepared by impregnation method. The physical and chemical properties will be characterized by the XRD and FTIR analysis whereas catalytic testing will be analyzed by *n*-dodecane and 1,4-diisoproylbenzene hydrocracking. The XRD results showed that the peak intensity of the tetragonal phase of ZrO_2 and bulk crystalline of Cr_2O_3 increased with the increase in the Cr_2O_3 loading from 1 to 12 wt%. The FTIR KBr analysis showed the presence of monoclinic and tetragonal phase of ZrO_2 and none or only negligible amount of coke formed during the reaction. The 2,6-lutidine adsorbed FTIR analysis showed that six bands located at 1675, 1660, 1650, 1640, 1630 and 1625 cm^{-1} corresponding to the Brønsted acid sites whereas the Lewis acid sites located at 1608, 1603, 1593, 1580, 1565 and 1560 cm^{-1}. For *n*-dodecane and 1,4-diisoproylbenzene hydrocracking, all catalysts showed 100% conversion except for Pt/12Cr_2O_3-ZrO_2. Hence, the presence of tetragonal phase and Lewis acid sites play an important role for catalytic activity of *n*-dodecane and 1,4-diisoproylbenzene hydrocracking.

1. Introduction

There has been a growing interest during the last few years in the catalytic cracking of hydrocarbon fuels due to the potential for enhancing engine performance over the entire spectrum of flight regimes. The development of alternative energy sources, such as biomass, solar and waste has attracted increasing attention due to global warming and the deficiency of fossil fuel [1]. Among them, various kinds of fuels can be synthesized via thermochemical processes of biomass. Gasification is a thermochemical process of biomass to produce syngas, which can be converted to liquid fuel through the Fischer–Tropsch process [2]. On the other hand, a hydroconversion process including hydrocracking or hydroisomerization, which reforms low quality fuel to high quality fuel, is essential because the Fischer–Tropsch process produces large molecular paraffins [3-4].

Fluid catalytic cracking (FCC) is one of the important processes to produce gasoline. It consists of various steps. Firstly, is the formation of carbenium ions. Then, different reactions proceed which include β-scission, isomerization, dealkylation, trans-alkylation, disproportionation, hydrogen transfer and others [5-6]. The cracking activity was determined by its Brønsted and Lewis acidity which catalyzes hydrocarbon cracking reaction via carbenium ion chemistry [7]. The interaction of protonic acid sites was generated from molecular hydrogen.

Chromium oxide catalysts have been used in many processes such as polymerization, hydrogenation, oxidation-reduction reactions. Cr_2O_3-ZrO_2 was found to be an active solid acid catalyst based on previous studies [3, 7-8]. The combination of ZrO_2 and Cr_xO_y generated stronger acid sites and more acidity as compared with the separate components. The presence of Pt loaded on Cr_2O_3-ZrO_2 promotes the catalytic activity and stability of Cr_2O_3-ZrO_2. While, zirconia have interesting thermal and mechanical properties which make it an important support material [8].

In this study, we focus on synthesis and characterization of Pt/Cr_2O_3-ZrO_2,-with different Cr_2O_3 loading; Pt/1Cr_2O_3-ZrO_2, Pt/4Cr_2O_3-ZrO_2, Pt/8Cr_2O_3-ZrO_2 and Pt/12Cr_2O_3-ZrO_2, and tested on the catalytic cracking of *n*-dodecane and1,4-diisopropylbenzene.

2. Experimental

2.1. Catalyst preparation

Zirconium hydroxide ($Zr(OH)_4$) was prepared by hydrolysis of aqueous solution of zirconium oxychloride ($ZrOCl_2{\cdot}8H_2O$) (Wako Pure Chemical) with 2.8 wt% NH_4OH aqueous solution [7-9]. Firstly, 50 g of zirconium oxychloride was dissolved with 2.5 L of double distilled water. NH_4OH solution (Merck) was then added up to pH 7 at 353 K with vigorously stirred and white colloidal precipitate was formed. The final pH was adjusted to 9 and the precipitated hydrogel was aged for 6 h at this temperature. The solution was decanted with deionized distilled water and the resulting slurry $Zr(OH)_4$, was filtered and washed with deionized water, and dried at 383 K for overnight.

The first supported chromium oxide zirconia, Cr_2O_3-ZrO_2 catalyst was prepared by impregnation method. The precursor used was chromium nitrate nonahydrate ($Cr(NO_3)_3{\cdot}9H_2O$, Merck) and zirconium hydroxide ($Zr(OH)_4$) as support. The support was pretreated with incipient volumes of solutions containing predetermined amounts of precursor were intimately mixed in order to prepare the catalyst. The resulting materials were dried overnight at 383 K followed by calcination at 873 K for 3 h and the content of Cr_2O_3 was varied for 1, 4, 8 and 12 wt%. Furthermore, Pt/Cr_2O_3-ZrO_2 catalyst was prepared by impregnation of Cr_2O_3-ZrO_2 with aqueous solution of hydrogen hexachloroplatinate hydrate ($H_2PtCl_6.6H_2O$, Aldrich) followed by drying overnight and calcination at 873 K for 3 h in air with the content of Pt was 0.5 wt% [3, 7-8].

2.2 Characterization

The XRD conducted using Bruker Advance D8 X-ray powder diffractometer with a Cu Kα (λ= 1.5418 Å) radiation was diffracted monochromatic beam at 40 kV and 40 mA. The data were collected at room temperature over the range of 2θ = 2-45° with scan rate of 0.025° continuously. The BET surface area of the samples were determined by N_2 adsorption-desorption isotherm using a Beckham Coulter SA 3100 at 77 K. 0.07 g of catalyst was outgassed at 573 K for 3 h before being subjected to N_2 adsorption. For FTIR KBr analysis, the catalyst powder (fresh catalyst and spent catalyst) was ground thoroughly

with KBr in a mortar and mounted between the die before it was pressed in hydraulic press (5000 psi) to form a thin, intact and transparent pellet. The pellet was put in a sample holder before the spectrum of the pellet was determined by using Agilent Technologies Carry 600 FTIR spectrometer. In the 2,6-lutidine adsorbed FTIR analysis, catalyst (0.07 g) was ground and pressed before placed in multi-purpose stainless IR cell with CaF_2 windows. Before the analysis, the catalyst was activated at 598 K for 3 h, followed by outgassing at 598 K for 3 h. The activated sample was exposed to 2 Torr of 2,6-lutidine at room temperature, followed by outgassing at 423 K.

2.3 Catalytic testing

Catalytic hydrocracking of *n*-dodecane and 1,4-diisopropylbenzene were carried out in a microcatalytic pulse reactor at 423-623 K under hydrogen stream. Prior to the reaction, 0.4 g of the catalyst was subjected to O_2 treatment (O_2 = 15 ml/min) at 673 K for 1 h, followed by H_2 reduction (H_2 = 15 ml/min) at 673 K for 3 h. Then, the reactor was cooling down to a reaction temperature under hydrogen stream. A dose of reactant (4.40 µmol of *n*-dodecane and 5.28 µmol of 1,4-diisopropylbenzene) were passed over the activated catalyst and the products were trapped at 77 K before being flash-evaporated into an online 6090N Agilent Gas chromatograph equipped with VZ7 packed Column and FID detectors. The intervals between doses were kept constant at 30 min.

The conversion of reactant ($X_{reactant}$), selectivity to particular product (S_i) and yield to particular product (Y_i) were calculated according to Eqs. (1), (2) and (3), respectively.

$$X_{reactant} = \frac{\sum A_i - A_{res\_reactant}}{\sum A_i} \times 100 \quad (1)$$

$$S_i = \frac{A_i}{\sum A_i - A_{res\_reactant}} \times 100 \quad (2)$$

$$Y_i = \frac{X_{reactant} \times S_i}{100} \quad (3)$$

Where A_i and $A_{res\_reactant}$ are corrected chromatographic area of particular compound and residual reactant.

3. Results and discussion

3.1 Physical properties of catalysts

The physical form of Pt/Cr_2O_3-ZrO_2 is in expected solid form and in dark green color. Figure 1 shows the XRD patterns of $Pt/1Cr_2O_3$-ZrO_2, $Pt/4Cr_2O_3$-ZrO_2, $Pt/8Cr_2O_3$-ZrO_2, and $Pt/12Cr_2O_3$-ZrO_2. The tetragonal phase of ZrO_2 is observed at 2θ = 30.24° [8]. While the peak at 2θ = 35.2° corresponded to the cubic phase of ZrO_2. In addition, the peaks at 2θ = 28.28° and 31.44° are attributed to the monoclinic phase of ZrO_2 [7-8]. It can be seen that the tetragonal phase of ZrO_2 and bulk crystalline of Cr_2O_3 at 2θ = 24-25° showed an increased in the peak intensity when the loading of Cr_2O_3 is increasing from 1 to 12 wt%. Ruslan et al.[9] reported that the insertion of MoO_3 in ZrO_2 will markedly develop the tetragonal phase and reduce the monoclinic phase of ZrO_2. Walendziewski et al. [10] reported that the higher the calcination temperature, the higher the tetragonal phase content of the zirconia oxides. They also stated that the content of both crystallographic forms, which are tetragonal and monoclinic phase, depends mainly on the applied support precursor.

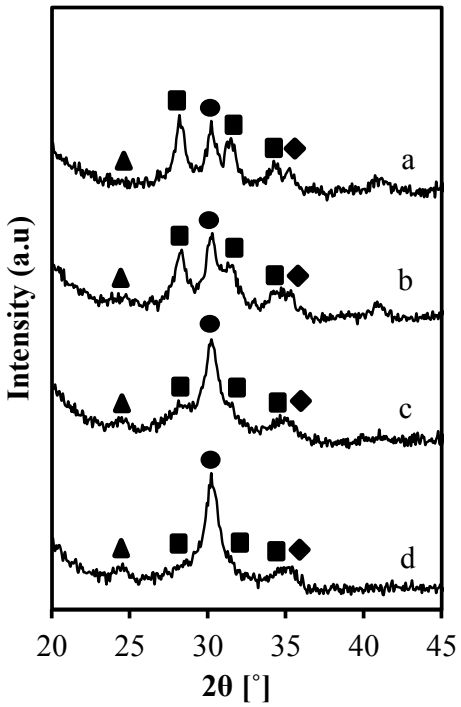

Figure 1.XRD patterns of Pt/Cr_2O_3-ZrO_2 with different Cr_2O_3 loading, (a) Pt/1Cr_2O_3-ZrO_2, (b) Pt/4Cr_2O_3-ZrO_2, (c) Pt/8Cr_2O_3-ZrO_2, and (d) Pt/12Cr_2O_3-ZrO_2, ( ) shows the tetragonal phase of ZrO_2, ( ) the bulk crystalline of Cr_2O_3, ( ) monoclinic phase of ZrO_2 and ( ) the cubic phase of ZrO_2.

Among all catalysts, Pt/8Cr_2O_3-ZrO_2 showed the highest BET surface area, which is 147 m^2/g. The BET surface area followed the order: Pt/8Cr_2O_3-ZrO_2 (147 m^2/g) > Pt/12Cr_2O_3-ZrO_2 (141 m^2/g) > Pt/4Cr_2O_3-ZrO_2 (89 m^2/g) > Pt/1Cr_2O_3-ZrO_2 (60 m^2/g). The increasing of Cr_2O_3 loading showed the increasing of the BET surface area of the catalysts. This is because of the increasing of tetragonal phase of ZrO_2 by the presence of Cr_2O_3 [3]. However, for Pt/12Cr_2O_3-ZrO_2, the Cr_2O_3 loading is too high until it formed an agglomeration of Cr_2O_3 on the surface and led to the decreasing of the BET surface area.

Figure 2 shows the FTIR spectra of Pt/1Cr_2O_3-ZrO_2, Pt/4Cr_2O_3-ZrO_2, Pt/8Cr_2O_3-ZrO_2, and Pt/12Cr_2O_3-ZrO_2 in the range of 400-4000 cm^{-1}. All FTIR spectra showed a broad band at 3450 cm^{-1} due to asymmetric stretching of the OH group. Two peaks were observed at 1631 cm^{-1} and 1411 cm^{-1} which corresponding to bending vibrations of –(H-O-H)- and -(O-H-O)- bonds. The peak at 505 cm^{-1} resulted from the presence of both tetragonal and monoclinic zirconia [11]. Zhou et al. [12] reported that the peaks in the 400-700 cm^{-1} regions resembled to the vibration of ZrO_2. The peaks at 424, 466 and 1060 cm^{-1} show the peaks for ZrO_2 [13]. An obvious decreased of the peak at 1060 cm^{-1} was observed for Pt/12Cr_2O_3-ZrO_2 which may due to the high loading of Cr_2O_3 on the ZrO_2 support.

Figure 3(A) and (B) show the fresh catalysts and spent catalysts for different Cr_2O_3 loading of Pt/Cr_2O_3-ZrO_2. FTIR KBr analysis gives the information on molecular vibrations and functional groups present,as well as the coke formation. The coke formation may lead to catalyst deactivation, plugging of the reactor and break down of the catalyst [14]. The spectra of fresh and spent catalysts did not show any apparent changes. Hence, it could be confirmed that all catalysts do not form any coke and carbonaceous species during the reaction.

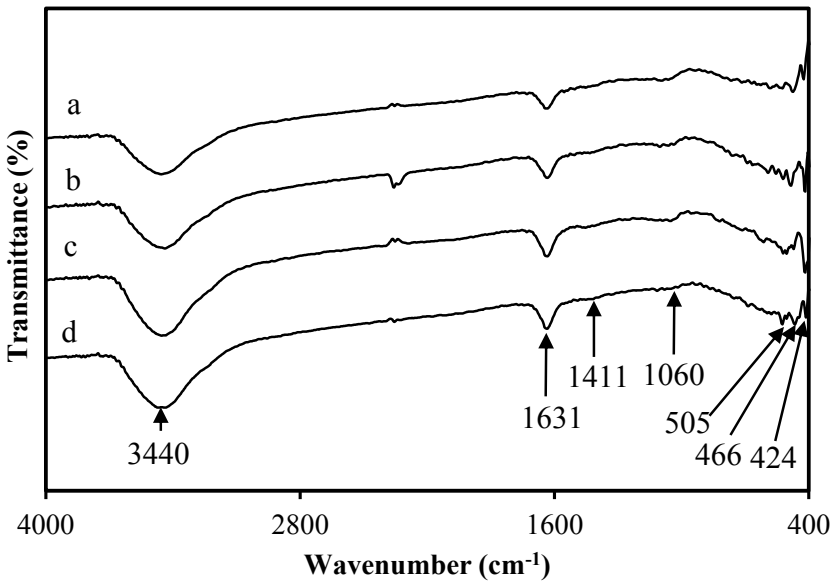

Figure 2. FTIR spectra of (a) Pt/1Cr_2O_3-ZrO_2, (b) Pt/4Cr_2O_3-ZrO_2, (c) Pt/8Cr_2O_3-ZrO_2, and (d) Pt/12Cr_2O_3-ZrO_2 in the region 400-4000 cm^{-1}.

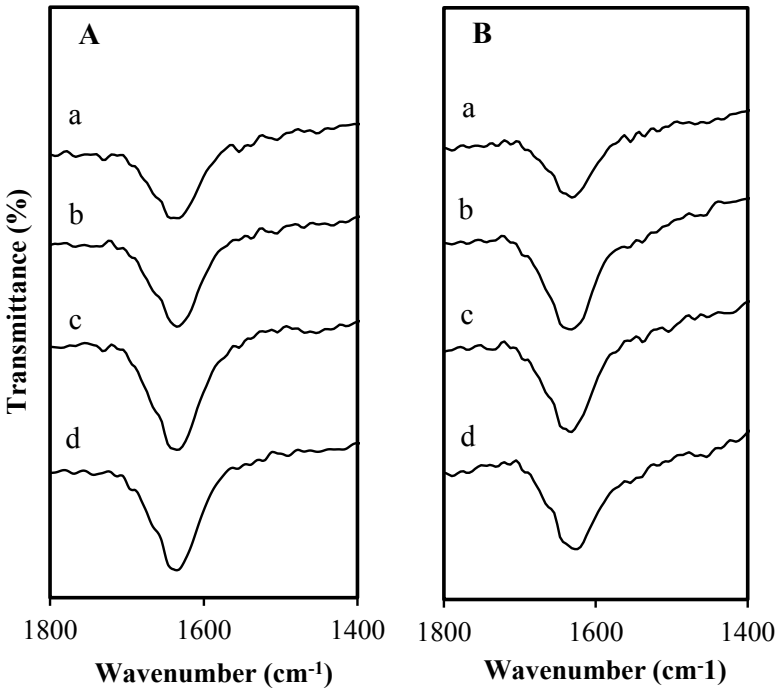

Figure 3. FTIR spectra of (A) fresh catalysts and (B) spent catalysts of (a) Pt/1Cr_2O_3-ZrO_2, (b) Pt/4Cr_2O_3-ZrO_2, (c) Pt/8Cr_2O_3-ZrO_2, and (d) Pt/12Cr_2O_3-ZrO_2.in the region 1400-1800 cm^{-1}.

3.2 Acidic properties of catalysts

The studies of infrared spectroscopic of 2,6-lutidine adsorbed on solid surfaces can distinguish between Brønsted and Lewis acids and to quantify the amounts independently. The catalysts were qualitatively probed by 2,6 –lutidine (pKb = 7.4) which is more basic than pyridine (pKb = 8.8) and is used to probe the relatively weak Brønsted acid sites and the acidic centers of Lewis acid sites due to the nature of the catalysts [15]. The use of 2.6-lutidine which is a strong base is known to be suitable for probing the Brønsted and Lewis acidic groups of ZrO_2 based-catalysts [7].

Fig 4(A) and (B) show the Brønsted acid sites and Lewis acid sites of different Cr_2O_3 loading of Pt/Cr_2O_3-ZrO_2 catalysts. As reported on previous studies, there were six bands located at 1675, 1660, 1650, 1640, 1630 and 1625 cm^{-1} corresponding to the Brønsted acid sites. As for Lewis acid sites, bands at 1608, 1603, 1593, 1580, 1565 and 1560 cm^{-1} were observed [3,8]. Strong doublet bands appeared at 1640 (8a mode) and 1630 (8b mode) cm^{-1} representing the protonated 2,6-lutidine species adsorbed on Brønsted acid sites. Shoulder bands at 1675 and 1660 cm^{-1} were due to the 8a and 8b ring vibrational modes, whereas the bands at 1650 (8a mode) and 1625 (8b mode) cm^{-1} were assigned to the 2,6-lutidinium ions of Brønsted acid sites [16]. With increase of Cr_2O_3 loading, doublets at 1650+1625, 1675+1660 and 1640+1630 cm^{-1} increased and reached maximum at 8 wt% Cr_2O_3 loading.

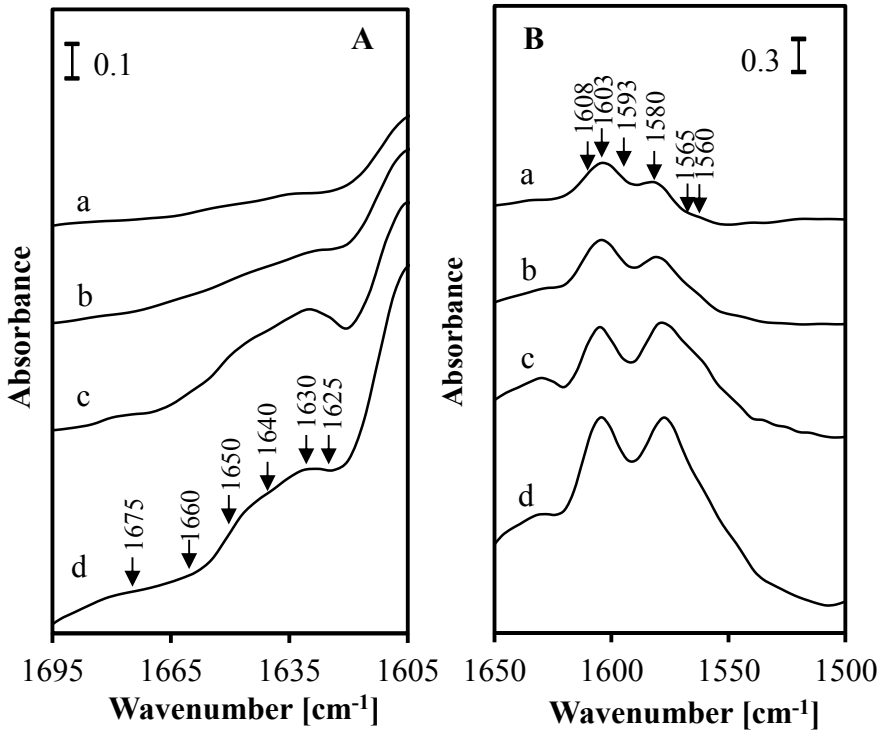

Figure 4. (A) IR spectra of 2,6-lutidine adsorbed on Brønsted acid sites of $Pt/1Cr_2O_3$-ZrO_2, $Pt/4Cr_2O_3$-ZrO_2, $Pt/8Cr_2O_3$-ZrO_2, and $Pt/12Cr_2O_3$-ZrO_2 in the region 1605-1685 cm^{-1}. (B) IR spectra of 2,6-lutidine adsorbed on Lewis acid sites of (a) $Pt/1Cr_2O_3$-ZrO_2, (b) $Pt/4Cr_2O_3$-ZrO_2, (c) $Pt/8Cr_2O_3$-ZrO_2, and (d) $Pt/12Cr_2O_3$-ZrO_2 in the region 1520-1640 cm^{-1}.

For the Lewis acid sites region, dual doublets were observed. The first was seen at 1608 (8a mode) and 1580 cm^{-1} (8b mode); the other was seen at 1593 (8a mode) and 1580 (8b mode) cm^{-1} indicating H-bonded 2,6-lutidine which corresponded to the monoclinic phase of ZrO_2. The doublet bands at 1608+1580 and 1593+1580 cm^{-1} slightly change in increasing of Cr_2O_3 loading. Furthermore, there were strong doublet bands corresponding to the tetragonal phase of ZrO_2 at 1603 (8a mode) and 1580 (8b mode) cm^{-1}. In addition, weak shoulder bands at 1565 (8a mode) and 1560 (8b mode) cm^{-1}

corresponding to the tetragonal phase of ZrO_2 were also observed [3,8,16]. Doublets at 1603+1580 cm^{-1} increased distinctly when increasing the Cr_2O_3 loading due to the formation of bulk species of Cr_2O_3 which consistent with the XRD results. Another Lewis acidic center at 1565+1560 cm^{-1} gave a slight decreased with the increase of Cr_2O_3 loading [8]. It shows that the Brønsted acid sites are weaker compared to Lewis acid sites for all catalysts. Pt/8Cr_2O_3-ZrO_2 showed the highest Brønsted acid sites compared to other catalysts. Meanwhile, Pt/12Cr_2O_3-ZrO_2 showed the highest Lewis acid sites.

3.3 Catalytic activity of catalysts

Figure 5(A) shows the conversion of *n*-dodecane hydrocracking for all Pt/Cr_2O_3-ZrO_2 catalysts. The Pt/1Cr_2O_3-ZrO_2, Pt/4Cr_2O_3-ZrO_2 and Pt/8Cr_2O_3-ZrO_2 showed 100 % conversion from 473 K to 623 K. Meanwhile, Pt/12Cr_2O_3-ZrO_2 gave conversion less than 3% at the temperature below 523 K. However, the conversion increased steeply to 61.3% at 573 K and continued increased to 82.9% at 623 K. These result showed that the higher the temperature of the reaction, the higher the conversion of *n*-dodecane. This may be due to the increase in the kinetic energy as the temperature increased [17-18]. Additionally, Pt/12Cr_2O_3-ZrO_2 showed the lowest conversion as compared to others. This is due to the agglomeration of Cr_2O_3 that may exist on the surface of the catalyst and lowering the catalytic activity of the catalyst [8]. This result is consistent with BET surface area analysis result in which there is a drop in BET surface area of Pt/12Cr_2O_3-ZrO_2.

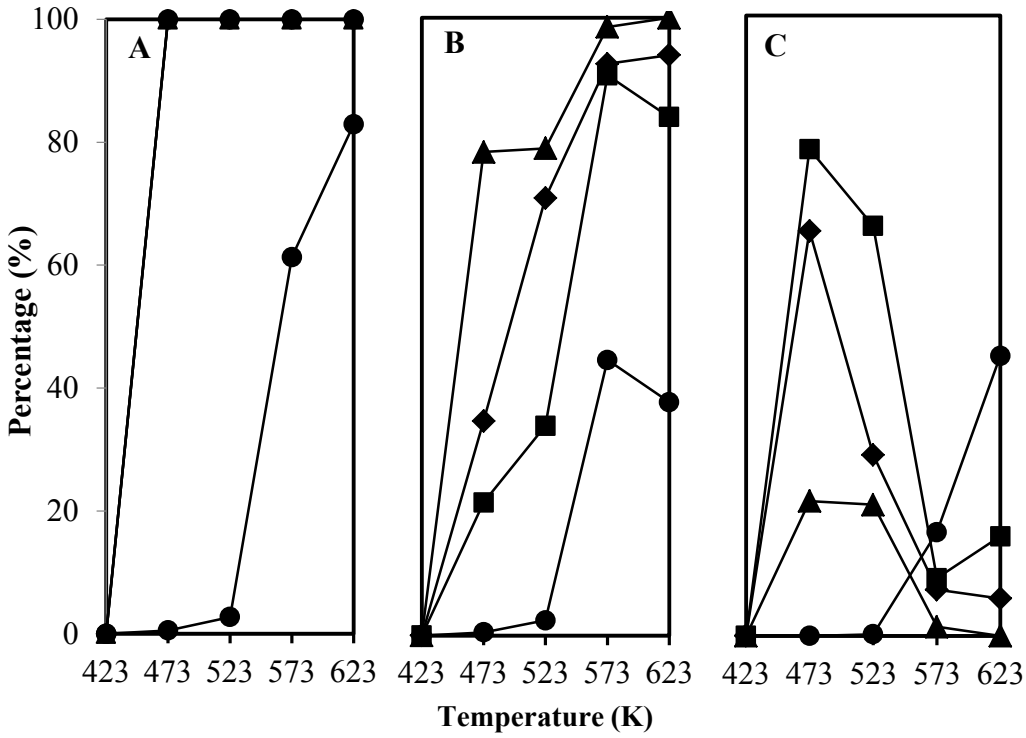

Figure 5. (A) The conversion, (B) yield of paraffin, and (C) yield of aromatic of *n*-dodecane hydrocracking for (■) Pt/1Cr_2O_3-ZrO_2, (▲) Pt/4Cr_2O_3-ZrO_2 , (◆) Pt/8Cr_2O_3-ZrO_2, and (●) Pt/12Cr_2O_3-ZrO_2.

Figure 5(B) shows the yield of paraffin products of the *n*-dodecane hydrocracking for all Pt/Cr_2O_3-ZrO_2 catalysts. The Pt/1Cr_2O_3-ZrO_2 yielded 3.6% of paraffin at 473 K, increase to 33.9% at 523 K and further increase to 90.7 % at 573 K. However, it decreased slightly to 83.9% at 623 K. This may be due to some coke formed that may be blocked the active sites of the catalyst. For Pt/4Cr_2O_3-ZrO_2, it showed a continuously increase in the yield of paraffin from 78.2% at 473 K to 100% at 623 K. Similarly, Pt/8Cr_2O_3-ZrO_2 also showed an increase in the yield of paraffin with the increase in the temperature. Pt/8Cr_2O_3-ZrO_2 yielded 34.7 % at 473 K and increased to 93.9 % at 623 K. As compared to others,

$Pt/12Cr_2O_3$-ZrO_2 showed the lowest yield of paraffin with less than 3 % at 473 K and increase to 44.6% at 573 K but decreased to 37.8% at 623 K.

Figure 5(C) shows the yield of aromatic products of the *n*-dodecane hydrocracking for all Pt/Cr_2O_3-ZrO_2 catalysts. $Pt/1Cr_2O_3$-ZrO_2 showed the highest yield of aromatics products as compared to other catalysts at 473 K. The yield of aromatic products showed optimum with 78.4% at 473 K followed by decreased to 9.3% at 573 K and slightly increased to 16.1% at 623 K. The $Pt/4Cr_2O_3$-ZrO_2 showed the yield of aromatic products decreased as the temperature increased. It showed 21.7 % at 473 K and fully diminished at 623 K. Similar pattern was observed for $Pt/8Cr_2O_3$-ZrO_2. At 473 K, it gave 65.2% of aromatics products and decreased to 29.1% at 523 K, and then, it further reduces to less than 10% at 623K. For $Pt/12Cr_2O_3$-ZrO_2, the yield of aromatics product from 473 K to 523 K is negligible. However, it increased to 16.7% at 573 K and further increased to 45.1% at 623 K.

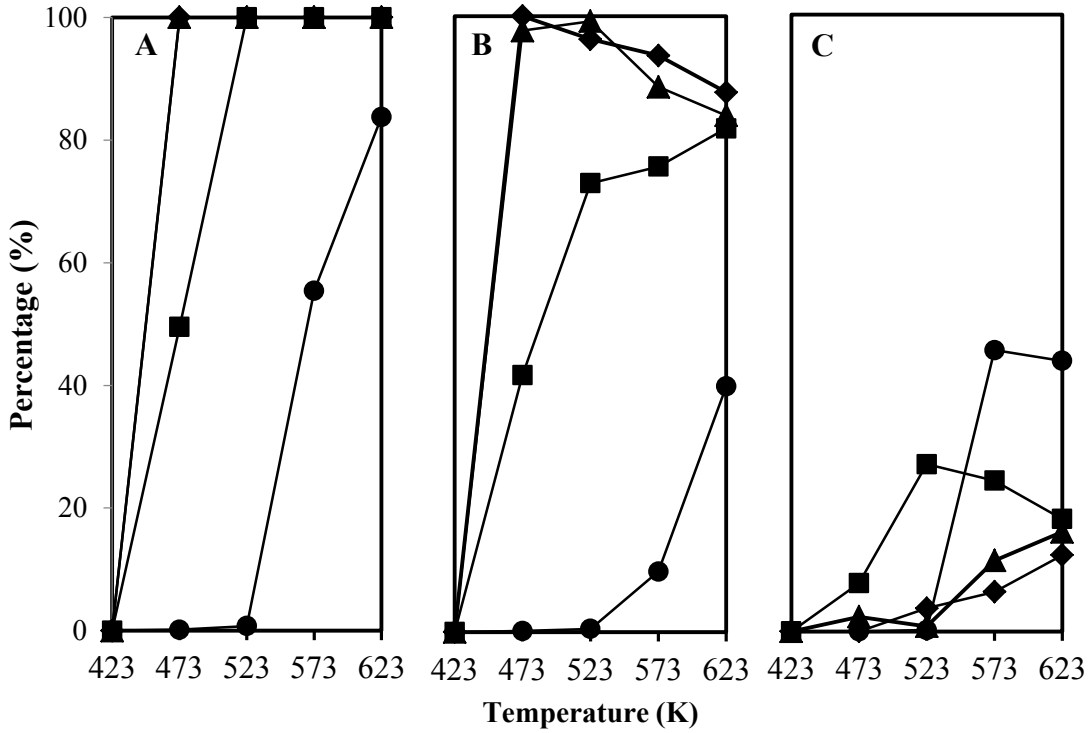

Figure 6. (A) The conversion, (B) yield of paraffin, and (C) yield of aromatic of 1,4-diisopropylbenzene hydrocracking for (■) $Pt/1Cr_2O_3$-ZrO_2, (▲) $Pt/4Cr_2O_3$-ZrO_2, (◆) $Pt/8Cr_2O_3$-ZrO_2, and (●) $Pt/12Cr_2O_3$-ZrO_2.

Figure 6(A) shows the conversion of the 1,4-diisopropylbenzene hydrocracking for all Pt/Cr_2O_3-ZrO_2 catalysts. The $Pt/4Cr_2O_3$-ZrO_2 and $Pt/8Cr_2O_3$-ZrO_2 showed 100 % conversion from the temperature 473 K to 623 K. Besides, $Pt/1Cr_2O_3$-ZrO_2 showed 49% conversion at 473 K and increased to 100 % conversion at 523 K to 623 K. However, $Pt/12Cr_2O_3$-ZrO_2 did not reach 100 % conversion in 1,4-diisopropybenzene hydrocracking. From 473 to 523 K, $Pt/12Cr_2O_3$-ZrO_2 having less than 1% conversion and it increased steeply to 55.4% at 573 K and 83.8% at 623 K. These results showed that as the temperature increased, the conversion of 1,4-diisopropylbenzene hydrocracking also increased.

Figure 6(B) shows the yield of paraffin products of the 1,4-diisopropylbenzene hydrocracking for all Pt/Cr_2O_3-ZrO_2 catalysts. For $Pt/1Cr_2O_3$-ZrO_2, the yield of paraffin is 41.7 % at 473 K and increased to 72.8 % at 523 K. The yield of paraffin continued increased to 75.5% at 573 K and 81.7% at 623 K On the contrary, $Pt/4Cr_2O_3$-ZrO_2 showed a different pattern as $Pt/1Cr_2O_3$-ZrO_2. At 473 K, the yield of paraffin is 97.6 % and increased slightly to 100% at 523 K. However, it decreased to 88.5% at 573 K and continued decreased to 83.8% at 623 K. In addition, $Pt/8Cr_2O_3$-ZrO_2 showed that the yield of paraffin decreased as the temperature increased. At 473 K, the yield was 100% and decreased to 87.6 %

at 623 K. Moreover, Pt/12Cr_2O_3-ZrO_2 showed that as the temperature increased, the yield of paraffin also increased. At 473 K-523 K, the yield of paraffin was less than 1 %. At 573 K, it increased to 9.8% and further increased to 39.8 % at 623 K.

Figure 6(C) shows the yield of aromatic products of the 1,4-diisopropylbenzene hydrocracking for all Pt/Cr_2O_3-ZrO_2 catalysts. The yield of aromatics products for Pt/1Cr_2O_3-ZrO_2 increased from 7.8% at 473 K to 41.4% at 573 K. However, it decreased to 18.2% at 623 K. It may be due to some of the aromatic products converted to paraffin products due to the ring opening of the aromatic. Pt/4Cr_2O_3-ZrO_2 showed that the yield of aromatic products was 2.4% at 473 K and slightly decreased to 0.8% at 523 K. However, the yield was increased back to 11.5% at 573 K and further increased to 16.1% at 623 K. Besides, Pt/8Cr_2O_3-ZrO_2 showed a constant increased in the yield of aromatics product from 523 K to 623 K but no any aromatics products were observed at 473 K. The highest aromatic yield obtained is 12.4% at 623 K. For Pt/12Cr_2O_3-ZrO_2, no yield of aromatic products was observed at 473 K. But, an obvious increased to 45.6% at 573K and it slightly decreased to 43.9% at 623 K was obtained.

The details of the paraffins and aromatics products of *n*-dodecane and 1,4-diisopropylbenzene hydrocracking reaction is shown in table 1. The paraffin products consist of methane, propane, hexane, cyclohexane and 3-methylhexane. On the other hand, the aromatic products consist of benzene, toluene, ethylbenzene, p-xylene and m-xylene.

Table 1 Details of paraffin and aromatic products.

Paraffin	Aromatic
Methane	Benzene
Propane	Toluene
Hexane	Ethylbenzene
Cyclohexane	p-xylene
3-Methylhexane	m-xylene

Conclusion

Pt/Cr_2O_3-ZrO_2 with different Cr_2O_3 loading (Pt/1Cr_2O_3-ZrO_2, Pt/4Cr_2O_3-ZrO_2, Pt/8Cr_2O_3-ZrO_2, and Pt/12Cr_2O_3-ZrO_2) were successfully synthesized using impregnation method. The XRD results showed the increase in the peak intensity of the tetragonal phase of ZrO_2 and bulk crystalline of Cr_2O_3 with the increase in the Cr_2O_3 loading. The BET surface area analysis showed that Pt/8Cr_2O_3-ZrO_2 possessed the highest BET surface area, which is 147 m^2/g. The FTIR KBr analysis showed that none or negligible amount of coke may be form on all catalysts during the reaction. The 2,6-lutidine adsorbed FTIR analysis showed that six bands located at 1675, 1660, 1650, 1640, 1630 and 1625 cm^{-1} corresponding to the Brønsted acid sites whereas the Lewis acid sites located at 1608, 1603, 1593, 1580, 1565 and 1560 cm^{-1}. All catalysts showed 100 % conversion except for Pt/12Cr_2O_3-ZrO_2 in 1,4-diisoproylbenzene and *n*-dodecane hydrocracking. The products consist of paraffin and aromatic. The paraffin products included methane, propane, hexane, cyclohexane and 3-methylhexane. On the other hand, the aromatic products included benzene, toluene, ethylbenzene, p-xylene and m-xylene. As the conclusion, the presence of Cr_2O_3 led to the increase in tetragonal phase and Lewis acid sites play a crucial role for catalytic activity of 1,4-diisoproylbenzene and *n*-dodecane hydrocracking.

Acknowledgments

This work was supported by the Universiti Teknologi Malaysia and Universiti Teknologi MARA under Research University Grants no. 13H61 and STG 07/UITM/02/23 under Ministry of Higher Education, Malaysia.

References

[1] Firmansyah M L, Jalil A A, Triwahyono S, Hamdan H, Salleh M M, Ahmad W F W and Kadja G T M 2016 *Catal. Sci. Technol.* **6(13)** 5178-5182
[2] Sahu R, Song B J, Im J S, Jeon Y P and Lee C W 2015 *J. Ind. Eng. Chem.* **27** 12-24
[3] Annuar N H R, Jalil A A, Triwahyono S and Ramli Z 2013 *J. Mol. Catal. A: Chem.* **377** 162-172
[4] Ishihara A, Tatebe K, Hashimoto T and Nasu H 2018 *Ind. Eng. Chem. Res.* **57(43)** 14394-14405
[5] Ajumobi O O, Muraza O, Bakare I A and Al Amer A M 2017 *Energ. Fuel.* ***31*****(11)** 12612- 12623
[6] Tukur N M and Al-Khattaf S 2005 *Chem. Eng. Process* **44(11)** 1257-1268
[7] Annuar N H R, Jalil A A, Triwahyono S, Fatah N A A, Teh L P and Mamat C R 2014 *Appl. Catal. A: Gen.* ***475*** 487-496
[8] Annuar N H R, Triwahyono S, Jalil A A, Basar N, Abdullah T A T and Ahmad A 2017 *Appl. Catal. A: Gen.* **541** 77-86
[9] Ruslan N N, Triwahyono S, Jalil A A, Timmiati S N and Annuar N H R 2012 *Appl. Catal. A: Gen.* **413** 176-182
[10] Walendziewski J, Pniak B, and Malinowska B 2003 *Chem. Eng. J.* **95(1-3)** 113-121
[11] Yang D, Li Y, Wang Y and Jiang Z 2014 *RSC Adv.* **4(91)** 49811-49818
[12] Zhao J, Xie J, Au C T and Yin S F 2014 *RSC Adv.* **4(12)** 6159-6164
[13] Sahu H R and Rao G R 2000 *B. Mater. Sci.* **23(5)** 349-354
[14] Son I H, Lee S J, Song I Y, Jeon W S, Jung I, Yun D J, Jeong DW, Shim J O, Jang W J and Roh H S 2014 *Fuel* **136** 194-200
[15] Timmiati S N, Jalil A A, Triwahyono S, Setiabudi H D and Annuar N H R 2013 *Appl. Catal. A: Gen.* **459** 8-16
[16] Onfroy T, Clet G and Houalla M 2005 *J. Phys. Chem. B* **109(8)** 3345-3354
[17] Lee H W, Jeon J K, Jeong K E, Kim C U, Jeong S Y, Han J and Park Y K 2013 *Chem. Eng. J.* **232** 111-117
[18] Ahmed M H, Muraza O, Jamil A K, Shafei E N, Yamani Z. H and Choi K H 2017 *Energ. Fuel.* **31(5)** 5482-5490